ISSN: 2634-9221
European Journal of Applied Sciences; Vol. 14 No. 03 (2026) (390-408)
https://doi.org/10.14738/ejas.1403.8934

Synthesis and Characterization of Composite Copper – Iron Nanoparticles from Copper Tailings using Sodium Borohydride as Reductant

Okpala-Chinonso, A. N., Moronkola, B. A., & Alegbe, M. J.

1. Department of Chemistry, Lagos State University

Abstract: The pollution caused by mine tailing, a leftover after excavating the useful mineral resources is often rich in metal ores that can be used as reagent to synthesize bimetallic or composite copper–iron nanoparticles (Cu–Fe NPs). The aim of this research is to synthesize and characterize composite Cu–Fe NPs synthesized from copper tailings. Experimental approach: Pulverized copper tailing (PCT) particles was digested and used as precursor copper reagent material with reagent iron salt solution to form Cu–Fe solution which was subjected to chemical reduction method. The synthesized composite Cu–Fe NPs was characterized using analytical techniques such as X-Ray Diffraction (XRD), Scanning Electron Microscopy (SEM), Transmission Electron Microscopy (TEM), etc. Results: The synthesized Cu–Fe NPs was optimized and characterized using 10 %, 20 %, 30 %, and 40 % of Fe content with the copper tailing solution. XRD showed well-defined crystalline phases corresponding to Cu and Fe oxides with crystallite sizes for 10 %, 20 %, 30 %, and 40 % of Fe to be 10 nm, 6 nm, 8 nm, and 8 nm respectively which varied slightly with the iron content which indicated that Fe incorporation influenced crystal growth and structural properties. SEM images revealed agglomeration, porous, and irregular particle structures across all the samples, while TEM confirmed predominantly spherical morphology with particle sizes of 10 %, 20 %, 30 % and 40 % Fe composition to be 7.2 nm, 3.2 nm, 5.4 nm and 5.3 nm respectively. FTIR identified O–H, CO2, C=O, etc. XRF confirmed copper and iron as the predominant elements in the Cu–Fe matrix. The optimization study revealed the 20 % Fe incorporation was the preferred formulation for the synthesis of Cu–Fe NPs. Conclusion: A suitable quality of bimetallic Cu–Fe NPs was synthesized from the copper waste material.

Keywords: Copper tailing, digestion, reagent iron salt, chemical reduction, and characterization

INTRODUCTION

The rapid development of nanotechnology has significantly transformed environmental engineering, advanced materials science, and sustainable chemistry in recent years. Metallic nanoparticles, particularly copper (Cu) and iron (Fe)-based nanomaterials, have attracted considerable attention due to their unique physicochemical properties, including high surface area-to-volume ratio, enhanced redox activity, tunable electronic configuration, and superior catalytic performance [1-2]. These distinctive properties enable nanoparticles to exhibit remarkable reactivity and efficiency in pollutant removal processes, making them highly promising materials for environmental remediation. In particular, Cu and Fe-based nanoparticles have demonstrated strong potential in wastewater treatment applications due to their ability to catalyze redox reactions, degrade persistent organic contaminants, and adsorb emerging pollutants from aqueous environments [3-4]. Consequently, the integration of these nanomaterials into wastewater treatment systems has been widely investigated as an innovative and sustainable strategy for addressing the increasing challenges associated with pharmaceutical and industrial wastewater pollution [5-**6].** Copper nanoparticles (Cu–NPs) have been extensively studied for their catalytic, antimicrobial, and photocatalytic properties. Noble metals such as silver and gold, copper are relatively inexpensive while still offering high catalytic efficiency and strong antimicrobial activity [7-8]. Cu-based nanomaterials have demonstrated strong activity in the degradation of dyes, antibiotics, and pharmaceutical compounds in aqueous systems [9-10]. However, large-scale application of Cu–NPs remains limited by the high cost of commercial precursors and the environmental footprint associated with conventional synthesis routes. Conventional physical and chemical synthesis methods often require expensive metal salts, high energy input, and toxic reducing or stabilizing agents, which can generate hazardous by-products and increase production costs [11-12]. Consequently, sustainable and low-cost precursor alternatives such as plant extracts, microorganisms, and agricultural wastes are increasingly being explored as environmentally benign routes for nanoparticle synthesis [13]. In parallel, global mining operations generate enormous volumes of mine tailings, which are finely ground waste materials remaining after mineral extraction. These tailings frequently contain residual quantities of economically valuable metals such as copper and iron [14-15]. Improper disposal of mine tailings poses serious environmental challenges, including acid mine drainage, heavy metal leaching, groundwater contamination, and ecological toxicity [16-17]. Rather than treating mine tailings solely as environmental liabilities, recent studies have emphasized their potential as secondary resource reservoirs within circular economy frameworks [18-20]. Valorization of mine tailings into functional nanomaterials represents a sustainable strategy that simultaneously addresses waste management challenges and reduces raw material dependency. Mining tailings, which are often considered environmentally hazardous wastes, contain significant amounts of recoverable metals such as copper, iron, nickel, and other minerals that can be transformed into valuable nanomaterials through sustainable extraction and synthesis processes [21-22]. This approach aligns with circular economy principles by converting mining waste into high-value nanomaterials while reducing environmental risks and dependence on virgin raw materials [22-23]. Hydrometallurgical recovery methods, particularly acid leaching, have been successfully employed to extract copper ions from mine waste streams [16, 24]. The recovered metal ions can subsequently serve as precursors for nanoparticle synthesis via chemical reduction or green synthetic pathways [1, 25]. Such an approach reduces reliance on high-purity commercial salts while promoting environmental sustainability. Moreover, synthesizing nanomaterials from waste-derived precursors aligns with global sustainable development goals by minimizing resource depletion and industrial waste accumulation [26-27]. Iron nanoparticles, particularly zero-valent iron (nZVI), have become one of the most widely applied nanomaterials for environmental remediation [28-29]. Their strong reducing potential enables degradation of chlorinated solvents, nitroaromatic compounds, heavy metals, and pharmaceutical residues [30-31]. The high reactivity of nZVI stems from its nanoscale dimension and electron-donating capability. Nevertheless, several technical limitations hinder their practical application, including particle agglomeration, rapid oxidation, and reduced long-term stability [28, 32]. These drawbacks reduce active surface area and catalytic efficiency over time. To overcome these challenges, researchers have increasingly focused on bimetallic and composite nanostructures. The integration of two metals within a single nanosystem often produces synergistic effects that enhance catalytic performance, structural stability, and electron transfer efficiency [33-34]. In Cu–Fe systems, galvanic coupling between Fe^0 and Cu^0 facilitates accelerated redox reactions. Iron acts as a sacrificial electron donor, while copper enhances catalytic selectivity and promotes efficient electron transfer [32,35]. Such synergistic interactions significantly improve contaminant degradation rates compared to monometallic nanoparticles. Recent investigations have demonstrated that Cu–Fe composite nanoparticles exhibit enhanced degradation efficiency toward antibiotic residues and dye pollutants in wastewater [36-37]. Additionally, surface-engineered Cu–Fe nanoparticles have shown improved resistance to oxidation and aggregation, thereby extending their functional lifespan in aqueous environments [38]. These findings underscore the importance of designing structurally integrated bimetallic nanomaterials for environmental applications. Pharmaceutical wastewater has emerged as a major environmental concern due to the presence of active pharmaceutical ingredients (APIs), endocrine disruptors, antibiotics, and other biologically active compounds that are resistant to conventional treatment processes [39-40]. Incomplete removal of such contaminants contributes to ecological toxicity and antimicrobial resistance proliferation. Advanced oxidation processes (AOPs) and catalytic nanomaterials have shown significant promise in addressing these limitations by generating highly reactive radical species capable of degrading persistent organic pollutants and pharmaceutical residues [41-42]. Copper-based nanomaterials can activate oxidants to generate reactive oxygen species (ROS), while iron nanoparticles facilitate Fenton-like reactions for hydroxyl radical production [43-44]. The combination of Cu and Fe within a composite structure can therefore enhance both reductive and oxidative degradation pathways due to synergistic redox interactions between the two metals, which facilitate electron transfer and promote the generation of reactive oxygen species in catalytic remediation processes [45-47]. From a sustainability standpoint, synthesizing copper nanoparticles from mine tailings while preparing iron nanoparticles from reagent-grade iron salts represents a hybrid approach that balances waste valorization with controlled synthesis precision [48-49]. Waste-derived copper reduces production cost and environmental impact by utilizing secondary metal resources, whereas reagent-grade iron salts provide controlled reaction conditions that ensure reproducibility and structural consistency in nanoparticle formation [49-51]. This strategy offers a scalable pathway toward environmentally responsible nanomaterial production [52]. The physicochemical properties of nanoparticles including size distribution, morphology, crystallinity, and surface chemistry are strongly influenced by synthesis methodology and reaction conditions [53-54]. Chemical reduction using sodium borohydride remains a widely adopted technique due to its strong reducing potential and its ability to produce nanoscale metallic particles with controlled size distribution [55-56]. For iron nanoparticles, co-precipitation followed by reduction under controlled atmospheric conditions ensures formation of zero-valent iron with minimized oxidation and enhanced stability [57-58]. Optimization of synthesis parameters such as pH, temperature, precursor concentration, and stirring rate is critical to achieving stable and uniformly dispersed nanoparticles [59-60]. Comprehensive characterization of synthesized nanomaterials is essential to validate structural and functional properties. X-ray diffraction (XRD) provides phase identification and crystallite size estimation. Scanning electron microscopy (SEM) and transmission electron microscopy (TEM) enable visualization of morphology and nanoscale dimensions. Fourier-transform infrared spectroscopy (FTIR) reveals surface functional groups, while energy-dispersive X-ray spectroscopy (EDX) confirms elemental composition and purity [61-62]. These techniques collectively ensure accurate assessment of synthesis efficiency and material quality. Despite increasing research on Cu–Fe nanocomposites, only limited studies have been specifically investigated on the integration of mine-tailing-derived copper with reagent-synthesized iron nanoparticles. Most existing work on Cu–Fe bimetallic systems has used commercially sourced high-purity reagent copper salts for controlled synthesis and structural stability [63-64]. Only a few studies have explored the synthesis of copper nanoparticles directly from mining tailings, demonstrating similar structural characteristics to conventionally synthesized materials and indicating potential for circular economy applications [49, 65]. Furthermore, the recent work on mineral-based synthesis of $CuFe_2O_4$ emphasizes the feasibility of using copper-rich ores, but this remains a nascent area of research [66]. There remains a knowledge gap regarding whether tailing-derived copper can achieve comparable structural integrity, crystallinity, and catalytic performance, highlighting the need for further investigation into waste-derived precursors for sustainable nanomaterial production [67-68]. Recent studies also emphasized that mine tailings contain valuable metals for nanoparticle synthesis, with their integration into advanced nanomaterial system remains underexplored and requires further research to optimize performance and scalability [69-70]. Therefore, the present study aim to synthesize composite Cu–Fe nanoparticles using digested copper extracted from copper mine tailings reagent-grade ferric chloride salt using sodium borohydride as the reductant. Cu–Fe is an alloy that has attracted a lot of interest not only due to their high strength and high electrical conductivity but also outstanding magnetic properties [71-73].

EXPERIMENTAL

Sample Collection and Sample Preparation

The collection of mine copper tailing was conducted in Dawa Town, Toro Local Government Area, Bauchi State and then taken to the laboratory for further analysis. The dried copper tailing was pulverized, and 10 g of the pulverized copper tailing (PCT) was digested with an aqua regia in ratio 3:1 of HNO_3 and HCl for 30 mins, the mixture solution was filtered into a 100 mL volumetric flask and made up to the mark with distilled water. Afterwards, the synthesis of Cu tailing-Fe nanoparticles was conducted by chemical reduction method.

Chemical and Reagent/Materials

Chemicals used in this research include HNO_3, HCl, $FeCl_3$, absolute ethanol; Cu tailings and all the reagents are used as received without further purification or treatment.

Synthesis of Composite Copper-Iron Nanoparticles

The crystal structure of the synthesized composite Cu--Fe nanoparticles from the mixture of copper tailings and ferric chloride solution mixture was conducted by chemical reduction method using [74-75] approach. The freshly prepared $NaBH_4$ solution was added drop wise into 100 mL of each mixture of digested copper tailing solution with 10 %, 20 %, 30 % and 40 % of ferric chloride ($FeCl_3$) salt solution to form green mixture solution. Subject these mixtures to constant stirring using magnetic stirrer for 1h until the black precipitates gradually formed turns to brownish colour. The mixture was filtered to collect the residue which was washed several times with distilled water to remove the traces of impurities attached to the residue. The filtered residue was oven dried at a regulated temperature of 80 ^oC for 1 hour and kept in a desiccator to cool before it was weighed and recorded. Repeat the drying, cooling, weighing and recording process until a constant weight was obtained. Subject the dried residue to grinding, ~~and~~ sieving before storing in a sampling bottle. The synthesized composite copper-Iron nanoparticle was subjected to characterization analysis.

$$Cu^{2+} + Fe^{3+} + 2\ BH_4^- \rightarrow Cu\text{-}Fe^0 + 2\ B_2H_2 \quad \text{...} \quad 1$$

$$4\ Cu^{2+} + Fe^{3+} + BH_4^- + 5\ H_2O \rightarrow 2\ Cu\text{-}Fe + B(OH)_3 + 2\ H_2 + 7\ H^+ \quad \text{..................} \quad 2$$

$$Cu + Fe^{3+} + 2\ O_2 \rightarrow CuO + Fe_2\ O_3 \rightarrow CuFe_2O_4 \quad \text{.................,.........} \quad 3$$

Analytical Techniques

Characterization

The synthesized copper-iron nanoparticles (Cu–Fe NPs)from copper mine tailing with reagent copper salt reaction with sodium borohydride was identified using XRD (D8 of Bruker) with Cu Kα radiation 1.5418 A°, operating voltage 40 kV, current 40 mA and step size 0.02° in 2θ scan to determine the crystallinity and mineral composition. The morphology of Cu–Fe was carried out using scanning electron microscopy (SEM) was used to scan the surface morphology of the samples with ZEISS GeminiSEM 360, and the transmission electron microscopy (TEM) was used to scan the internal surface morphology of the synthesized Cu-Fe NPs with Hitachi HT7800 Series (120 kv TEM). X-Ray Fluorescence (XRF) was used to determine the elemental composition of the synthesized Cu–Fe NPs with Bruker-S1 TITAN (Handheld), Fourier Transform Infrared (FTIR) Spectroscopy was used to identify the functional groups in the Cu–Fe NPs with Bruker ALPHA II FTIR, Thermal properties of the synthesized Cu–Fe samples were analyzed by Thermo Gravimetric analysis (TG/DTA, Model Q600 SDT and Q20 DSC). BET was used to analyze the surface area of the synthesized copper tailing-iron nanoparticles with NOVA 1000e/4200e.

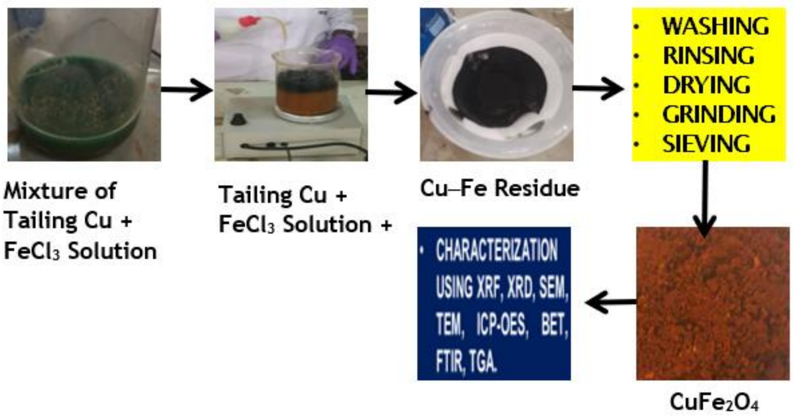

Figure 1: Experimental flow chart

RESULTS AND DISCUSSION

Characterization of Synthesized Copper-Iron Nanoparticles

XRD

The X- ray diffraction (XRD) results of the synthesized composite Cu–Fe nanoparticles at 10 %, 20 %, 30 % and 40 % Fe are presented in Figures 2-5 revealed tiny peaks of spectra which indicate crystallinity. At 10 % Fe loading with Cu being the dominant component revealed: Strong Cu peaks, minimal Fe contribution, and limited synergistic effect and it indicate strong Cu peaks with minimal Fe contribution, and limited synergistic effect.

At 20 % Fe loading, the XRD revealed a balanced mineral phase composition was observed to be characterized by dominant Cu peaks with emerging Fe phases and with slight peak broadening, which indicate a reduced crystallite size, enhanced dispersion and more active sites. The 20 % of Fe can form smaller crystallite size, with better dispersion and more active sites. "The 20 % Fe was the optimal because it had more Cu than Fe" composition. The optimal 20 % Fe is due to: synergistic Cu–Fe interaction, improved surface area from peak broadening, maintained Cu activity not because "Cu was more than Fe. At 20 % Fe, the XRD showed: moderate peak intensity with good crystallinity, peak broadening, smaller particle size with higher surface area. There was no excessive Fe oxide dominance with Cu sites still accessible. The 20 % Fe is a balanced mineral phase composition which is often revealed as optimal as Cu peaks are still dominant, and the Fe peaks appeared but not overwhelming, peak broadening showed slight shift with interaction between Cu and Fe. 20 % of Fe in the Cu–Fe NPs can form smaller crystallite size, better dispersion and more active sites. "The 20 % Fe is optimal because it has more Cu than Fe" "The 20 % Fe composition exhibited optimal performance due to a balanced Cu–Fe interaction, where Cu remained the dominant active phase while Fe contributed to enhanced surface properties and catalytic activity without excessive site blockage."

At 20 % Fe loading, the XRD revealed a balanced mineral phase composition was observed to be characterized by dominant Cu peaks with emerging Fe phases and with slight peak broadening, which indicate a reduced crystallite size, enhanced dispersion and more active sites. "The 20 % Fe was the optimal because it had more Cu than Fe" composition to form smaller crystallite size with better dispersion and more active sites. The optimal 20 % Fe is due to: synergistic Cu–Fe interaction, improved surface area from peak broadening, maintained Cu activity not because "Cu was more than Fe. At 20 % Fe, the XRD showed: moderate peak intensity with good crystallinity, peak broadening, smaller particle size with higher surface area. There was no excessive Fe oxide dominance with Cu sites still accessible. The 20 % Fe is a balanced mineral phase composition which revealed the optimal as Cu peaks are still dominant, and the Fe peaks appeared but not overwhelming, peak broadening showed slight shift with the interaction between Cu and Fe. 20 % of Fe in the Cu–Fe NPs can form smaller crystallite size, better dispersion and more active sites. "The 20 % Fe is optimal because it has more composition of Cu than Fe" "The 20 % Fe composition exhibited optimal performance due to a balanced Cu–Fe interaction, where Cu remained the dominant active phase while Fe contributed to enhanced surface properties and catalytic activity without excessive site blockage." The Figure 3 revealed the incorporation of Fe into the Cu lattice resulted in noticeable variations in peak broadening and the intensity to show the changes in crystallite size and structural properties. A significant reduction in the particle size was observed for 20 % Fe, which corresponds to the highest degree of peak broadening. The incorporation of Fe at this stage will enhance nucleation which effectively suppresses the crystal growth to form finer nanoparticles with increased surface area.

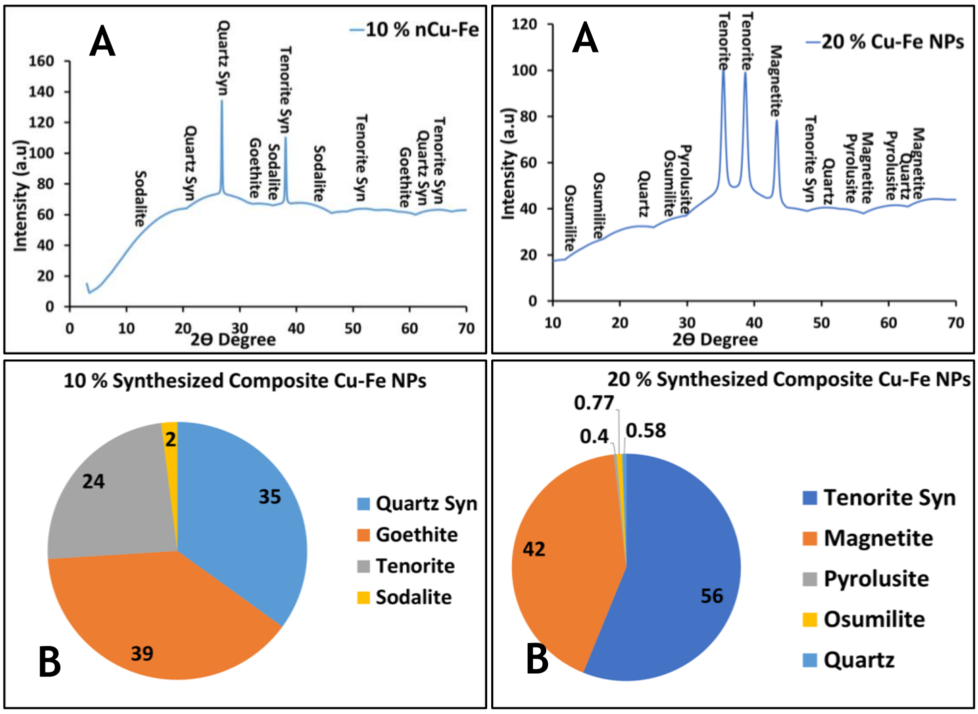

Figure 2: XRD spectra (A) and mineral composition (B) analysis of 10 % and 20 % Fe in synthesized Cu-Fe NPs

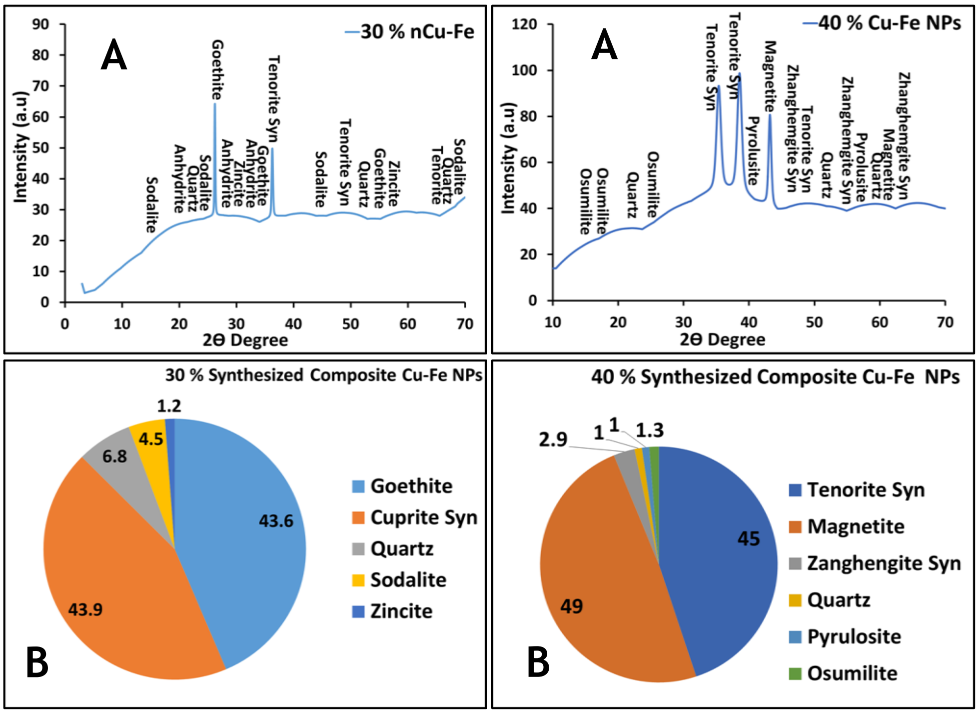

Figure 3: XRD spectra (C) and mineral composition (D) analysis of 30 % and 40 % Fe in synthesized Cu-Fe NPs

At 30–40 % Fe loadings, this structural configuration may likely contribute to the superior adsorption performance observed, as excess Fe content at higher loadings of 30–40 % Fe with Fe being dominant may give strong Fe oxide peaks, reduced Cu signal with possible agglomeration, partial blockage of active Cu sites and reduced adsorption efficiency.” This structural configuration may likely contribute to the superior adsorption performance observed as excessive Fe content at higher loadings 30–40 % Fe and could lead to agglomeration, partial blockage of active Cu sites and reduced adsorption efficiency.” The XRD analysis revealed that increasing % Fe content will alter the crystalline structure of the Cu–Fe nanoparticles.

The crystallite sizes calculated using Scherrer’s equation for the 10 %, 20 %, 30 %, and 40 % Fe compositions were 10 nm, 6 nm, 8 nm, and 8 nm respectively but smaller in size than the one reported in [76]. Fe compositions at 30 % and 40 % will cause a slight increase and stabilization in the crystallite size (8 nm) observed, accompanied by relatively reduced peak broadening compared to the 20 % Fe sample [77]. This indicates that 20 % Fe was the optimum and any further addition of Fe beyond the optimal level (20 % Fe) does not significantly enhance the size reduction, possibly due to the initial particle interaction, with partial agglomeration to cause reduction in the lattice distortion [77-79]. Increasing the Fe content will cause lattice strain and possible substitution of Cu ions to confirm successful incorporation of Fe into the Cu matrix [77]. The X-ray diffraction (XRD) mineral phase composition results of 10 %, 20 %, 30 % and 40 % Fe composition for the synthesized impregnated Cu–Fe nanoparticles in Figures 2-5 confirmed the formation of tiny peaks revealing crystallinity with mineral phases that are characteristic to copper and iron. The mineral phases for 10 % Fe and 30 % Fe composition were both goethite but the Cu mineral phases in the samples, consist of Tenorite for 10 % and Cuprite for 30 % Fe the synthesized Cu–Fe NPs [48, 77, 80]. The mineral phases for 20 % Fe and 40 % Fe of synthesized Cu–Fe NPs consist of the same mineral phase compositions for both Cu and Fe to be Tenorite and Magnetite respectively.

SEM AND TEM

Scanning Electron Microscopy (SEM) presented in Figure 4 was used to investigate the surface morphology of the synthesized Cu–Fe nanoparticles. The SEM images of the synthesized Cu–Fe nanoparticles revealed spherical irregular particle sizes with some agglomeration. The particles appear clustered which could be due to strong inter-particle interactions and magnetic effects caused by iron. The surface morphology is rough and porous but very good for adsorption processes because it provides more active sites for interaction with some wastewater impurities. The TEM morphology presented in Figure 5 is used to investigate the inner morphology of the synthesized Cu–Fe NPs. The TEM morphology for the synthesized Cu–Fe NPs are spherical with irregular shape with partially dispersed particle sizes. `TEM particle sizes of the synthesized impregnated Cu–Fe nanoparticles of the results of 10 %, 20 %, 30 % and 40 % Fe composition was calculated using Imagej software to be 7.2 nm, 3.2 nm, 5.4 nm and 5.3 nm respectively. The TEM particle sizes for 10 %, 20 %, 30 % and 40 % Fe composition for the synthesized impregnated Cu–Fe nanoparticles revealed similar pattern to the Scherer’s particle size calculated results.

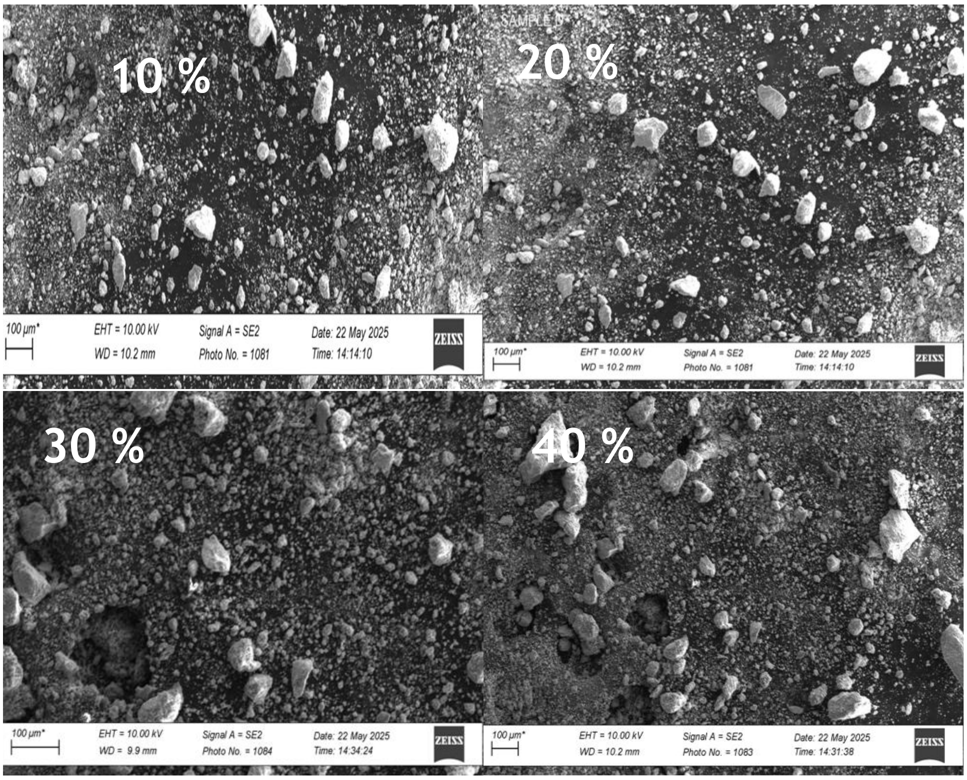

<u>Figure 4</u>: SEM morphology 10 %, 20 %, 30 % and 40 % Fe of synthesized composite Cu-Fe NPs

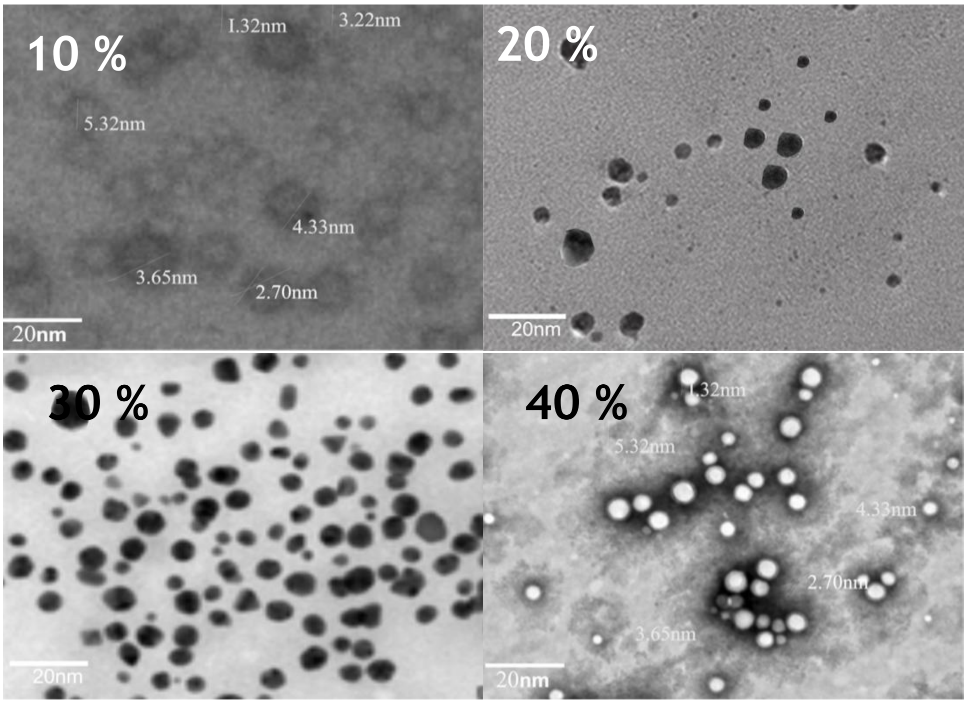

<u>Figure 5</u>: TEM morphology 10 %, 20 %, 30 % and 40 % Fe in synthesized composite Cu-Fe NPs

FTIR

FTIR Analysis:

Fourier-transform infrared (FTIR) spectroscopy provides insight into the surface chemistry and functional groups of the nanoparticles in the samples presented in Figure 6. The FTIR spectra of the synthesized Cu-Fe nanoparticles of 10 %, 20 %, 30 % and 40 % Fe revealed broad absorption bands O-H stretching at 3283.79 cm^{-1}, sharp short peak bands of C-H stretching at 2903.60 cm^{-1} for 20 % and 40 % while that of 10 % and 30 % were not conspicuous. Absorption peaks at 2266.22 cm^{-1} and 2053.76 cm^{-1} revealed the presence of CO_2 for all the samples. Peaks observed near 1625.76 cm^{-1} is associated with the asymmetric vibration of the carbonyl group while the weaker band at 1475.15 cm^{-1} describes the symmetric vibration of the carbonyl group in the free carboxylic group 1475.15 cm^{-1} correspond to O–H stretching and bending respectively [81]. The FTIR absorption bands at 1103.29 cm^{-1} can be attributed to the presence of C–O bond [76, 82-83]. The characteristic metal–oxygen vibration bands detected in the region 600-700 cm^{-1} are assigned to Cu-O and Fe–O stretching vibrations to confirm the formation of composite copper–iron oxide ($CuFe_2O_4$) nanoparticles [84].

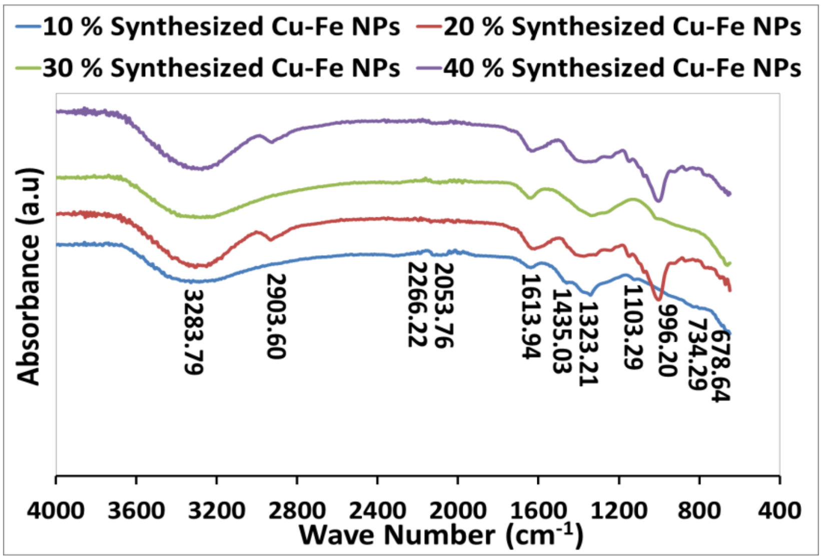

Figure 6: FTIR analysis of 10 %, 20 %, 30 % and 40 % Fe in synthesized composite Cu-Fe NPs

XRF

The X-ray fluorescence (XRF) analysis of the synthesized Cu-Fe nanoparticles at 10 %, 20 %, 30 % and 40 % Fe presented in Figure 7 confirmed the presence of copper and iron as the major elements as seen in Figures 2-3. The elemental composition of the synthesized Cu-Fe nanoparticles varied with the % Fe precursor concentration. The 20 % Fe-doped sample exhibited a balanced Cu-Fe composition with a higher proportion of copper compared to other samples, which is favorable for adsorption and catalytic activity. XRF elemental composition results with the XRD crystal structure combine to validate the synthesis of Cu-Fe NPs. It explains that: addition of Fe improves the magnetic properties, catalytic activity, and high amount of Cu gives better adsorption properties. The improved performance of the 20 % Fe synthesized Cu-Fe NPs can be attributed to its optimal Cu-Fe ratio, as confirmed by XRF elemental analysis and it provides sufficient active copper sites while maintaining the synergistic effect of iron. Trace elements such as Si, Al, and Ca were also detected, which was likely to originate from the mine tailings used as precursor materials. These impurities were minimal and did not significantly affect nanoparticle performance. The results confirmed successful synthesis due to the presence of both Cu and Fe which proves formation of composite nanoparticles. XRF revealed the elemental composition of the nanoparticles, showing a consistent increase in Fe content was proportional to the intended doping levels. The Cu-to-Fe ratio measured by XRF corroborated the nominal compositions used in synthesis, confirming successful doping and homogeneity of the bimetallic system. These results complement the XRD data, validating that structural changes observed with increasing Fe are due to controlled elemental incorporation rather than impurities.

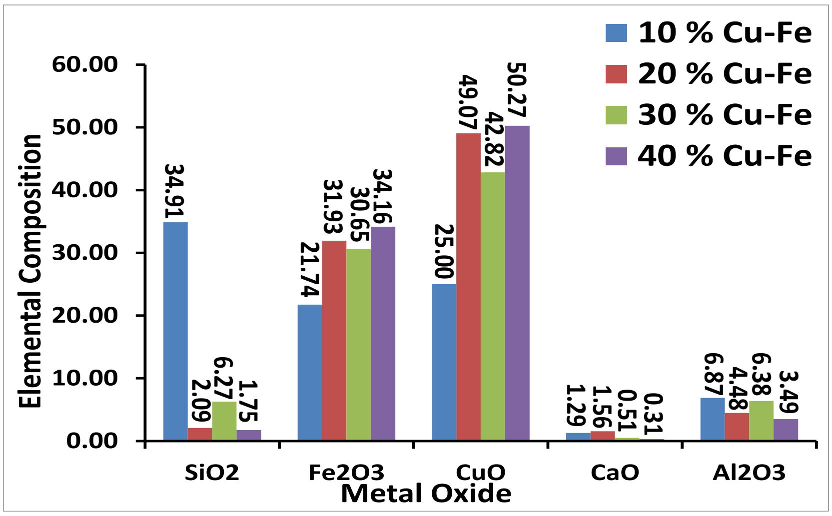

Figure 7: XRF elemental composition of 10 %, 20 %, 30 % and 40 % of Fe in synthesized composite Cu-Fe NPs

TGA

The thermogravimetric analysis (TGA) of the synthesized 20 % Fe composite Cu-Fe nanoparticle in Figure 8 revealed the TGA/DTA curves of the revealed a multi-stage weight loss pattern. composite Cu-Fe nanoparticles. TGA was conducted by heating 100 g of the Cu-Fe samples at the rate of 5 °C/minute and the samples exhibited two distinct stages of weight loss. The initial sharp weight loss from room temperature to 320 °C is due to evaporation of physisorbed water molecules while the second stage of a small weight loss at temperatures between 380 °C and 460 °C can be ascribed to the evaporation of chemisorbed water molecules [85]. Gradual weight loss up to 460°C is associated with the oxidation and structural transformation of the nanoparticles. At temperature above 600°C, there was no significant weight loss observed, which indicate the formation of thermally stable Cu-Fe oxide phases. The overall low weight loss confirms the high thermal stability of the synthesized composite Cu-Fe nanoparticles [86]. As the temperature rise above 460 °C, the TGA curve becomes flat which indicate that there was no significant weight loss was observed, which indicate the formation of thermally stable Cu-Fe oxide phases [84].

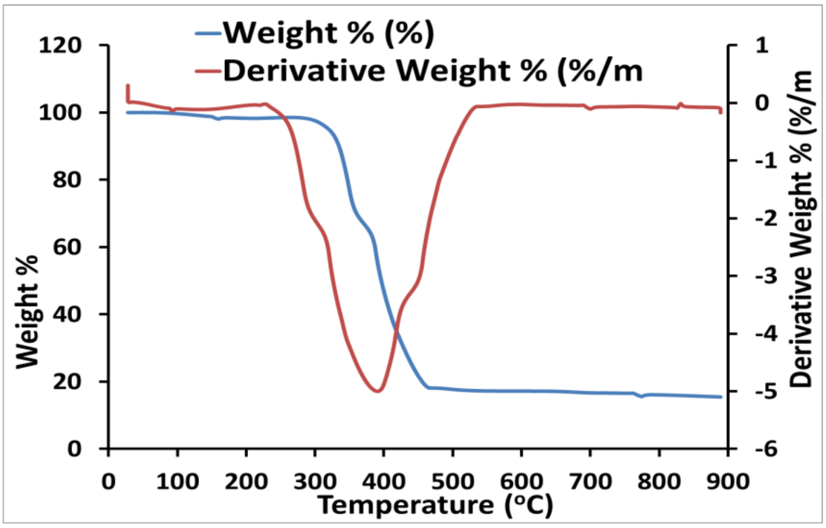

Figure 8: TGA/DTA analysis of synthesized composite Cu-Fe NPs

BET

The BET micropore of the synthesized Cu–Fe NPs from the mixture of mine tailings and reagent Fe salt sample are presented in Figure 9. Figure 9A revealed DA plot consisting of micropore volume and pore diameter to be 0.151 cc/g and 2.94 nm respectively. The pore size distribution in Figure 9B revealed the cumulative pore volume and cumulative surface area to be 0.066 cc/g and 669 m^2/g respectively. Langmuir isotherm and multipoint BET surface area results are presented in Figure 10. Figure 10A revealed the Langmuir isotherm surface area to be 979.67 m^2/g, which almost form a linear graph. Figure 10B presents the multi-point BET surface area to be 303.38 m^2/g revealed that the gas molecules formed a uniform layer on the surface of the adsorbent to make adsorption to occur in a monolayer form. The multipoint BET surface area depends on what it would be used for such as adsorbent, electronics, photonics, catalysis, semiconductor and biomedicine because of it's large surface area [77, 87-89]. The BET of the synthesized Cu–Fe NPs is higher than that of synthesized tailing Cu-NPs and reagent Cu-NPs reported by Okpala et al., (2026)[74].

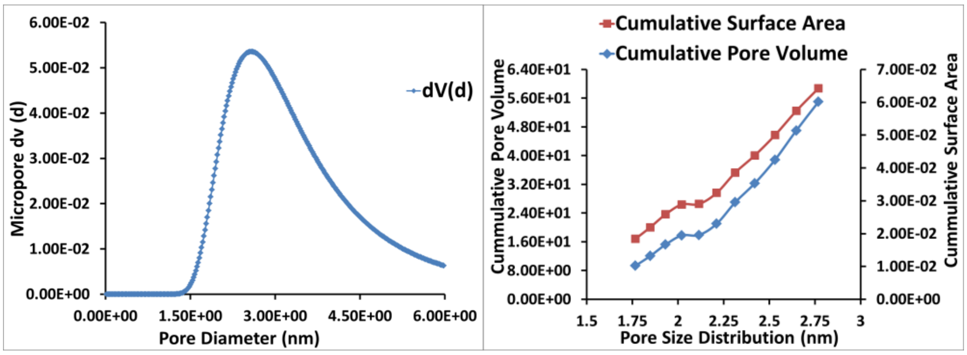

Figure 9: BET micropore (A) and pore size distribution (B) analysis of 20 % of synthesized composite Cu-Fe NPs

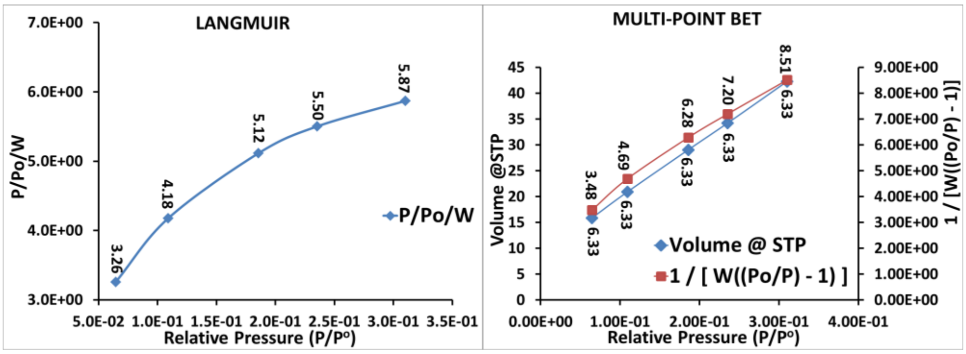

Figure 10: BET Langmuir (A) and Multi-point BET (B) analysis of synthesized composite Cu-Fe NPs

Acknowledgments

The authors wish to acknowledge the assistance of Mrs. Omowonuola, A.A, and Mr. Onifade, O.O who provided some technical supports and the Lagos State University created the enabling environment for the successful research to be conducted.

Funding

This research was funded by the authors only.

Conflict of Interest

The authors declare no conflicts of interest.

REFERENCES

1. Nasrollahzadeh, M., Sajjadi, M., Sajadi, S. M., & Issaabadi, Z. (2020). An introduction to copper nanoparticles: Synthesis and environmental applications. Environmental Research, 191, 110184. https://doi.org/10.1016/j.envres.2020.110184
2. Das, S., Dutta, S., & Pal, S. (2021). Metal and metal oxide nanoparticles in wastewater treatment: A review. Environmental Nanotechnology, Monitoring & Management, 15, 100447. https://doi.org/10.1016/j.enmm.2021.100447
3. Rashid, M., Khan, S., & Ahmad, I. (2024). Recent advances in the adsorption of pollutants from wastewater using carbon-based and metal-oxide nanoparticles. Applied Sciences, 14(24), 11492. https://doi.org/10.3390/app142411492
4. Al-Maqdi, K., Abdullah, M., & Rahman, N. (2025). Integration of used water filters and immobilized bimetallic iron-copper nanoparticles for rubber wastewater treatment. Separation and Purification Technology, 379, 135039. https://doi.org/10.1016/j.seppur.2025.135039
5. Tripathy, J., Mishra, A., Pandey, M., Thakur, R. R., Chand, S., Rout, P. R., & Shahid, M. K. (2024). Advances in nanoparticles and nanocomposites for water and wastewater treatment: A review. Water, 16(11), 1481. https://doi.org/10.3390/w16111481
6. Nkosi, N. C., Basson, A. K., Ntombela, Z. G., Dlamini, N. G., & Pullabhotla, R. V. S. R. (2024). A review on bioflocculant-synthesized copper nanoparticles: Characterization and application in

wastewater treatment. Bioengineering, 11(10), 1007. https://doi.org/10.3390/bioengineering11101007

7. Al-Kattan, A., Al-Gharrawi, M., & Mohammed, A. (2020). Copper nanoparticles: Green synthesis, characterization, and application in wastewater decontamination. Journal of Water Process Engineering, 38, 101615. https://doi.org/10.1016/j.jwpe.2020.101615.
8. Tabassum, S., Hossain, M. S., Saeed, M. A., Uddin, M. N., & Ahmed, S. (2025). Exploration of antibacterial and photocatalytic properties of CuO nanoparticles synthesized from plant extract and waste copper sources. Materials Advances, 6, 2338–2355. https://doi.org/10.1039/D4MA01047G
9. El-Aziz, M. A. A., Hassan, M. A., & El-Sayed, G. O. (2020). Copper nanoparticles for photocatalytic removal of pharmaceuticals from water: Efficiency and mechanisms. Scientific Reports, 10, 2222. https://doi.org/10.1038/s41598-020-59020-0
10. Wang, Z., Li, Y., & Zhang, T. (2022). Application of Cu–Fe oxide nanoparticles for photocatalytic degradation of pharmaceutical residues in real wastewater. Journal of Environmental Chemical Engineering, 10(4), 107801. https://doi.org/10.1016/j.jece.2022.107801
11. Rahman, M., Rahman, M. S., & Hasan, M. (2025). Green synthesis of nanomaterials: A review of sustainable production strategies. Journal of Research in Technology and Engineering, 6(3), 214–225.
12. Patiño-Ruiz, D., Martínez-Hernández, A. L., & Velasco-Santos, C. (2026). Sustainable approaches for the synthesis of metallic nanoparticles: Environmental implications and future perspectives. Journal of Cleaner Production, 435, 141068. https://doi.org/10.1016/j.jclepro.2025.141068
13. Malik, A. Q., Mir, T. U. G., Kumar, D., Mir, I. A., Rashid, A., Ayoub, M., & Shukla, S. (2023). A review on the green synthesis of nanoparticles, their biological applications, and photocatalytic efficiency against environmental toxins. Environmental Science and Pollution Research, 30, 69796–69823. https://doi.org/10.1007/s11356-023-27437-9
14. Choi, S., Kim, J., & Lee, W. (2022). Valorization of mining waste for nanomaterial synthesis: An emerging route for sustainable environmental remediation. Resources, Conservation & Recycling, 177, 105995. https://doi.org/10.1016/j.resconrec.2021.10599516
15. Sahoo, S. C., Das, B., & Mishra, B. K. (2021). Evaluation of mine waste valorization for synthesis of functional nanomaterials. Journal of Materials Research and Technology, 13, 2830–2844. https://doi.org/10.1016/j.jmrt.2021.05.045
16. Lottermoser, B. G. (2020). Mine wastes: Characterization, treatment and environmental impacts (4th ed.). Springer. https://doi.org/10.1007/978-3-030-34305-3
17. Santibáñez, C., Verdugo, C., & Ginocchio, R. (2021). Phytostabilization of copper mine tailings: A review of the state of the art. Science of the Total Environment, 789, 147–163. https://doi.org/10.1016/j.scitotenv.2021.147888
18. Binnemans, K., Jones, P. T., Blanpain, B., Van Gerven, T., Yang, Y., Walton, A., & Buchert, M. (2020). Recycling of rare earths: A critical review. Journal of Cleaner Production, 51, 1–22. https://doi.org/10.1016/j.jclepro.2019.118963
19. Zhang, L., Sun, W., & Hu, Y. (2021). Reprocessing of mine tailings: A review of environmental and economic implications. Minerals Engineering, 170, 107040. https://doi.org/10.1016/j.mineng.2021.107040

20. Edraki, M., Baumgartl, T., Manlapig, E., Bradshaw, D., Franks, D. M., & Moran, C. J. (2019). Designing mine tailings for better environmental, social and economic outcomes: A review of alternative approaches. Journal of Cleaner Production, 84, 411–420. https://doi.org/10.1016/j.jclepro.2014.04.079

21. Keskin, T., Yilmaz, E., Sari, M., Kasap, T., & Cao, S. (2026). Reuse and valorization practices of mine tailings: A review of existing perspectives and advances. Clean Technologies and Environmental Policy, 28, 103.

22. Reddy, P. V., & Kumar, A. (2024). Unlocking the potential: Mining tailings as a source of sustainable nanomaterials. Renewable and Sustainable Energy Reviews, 194, 114665. https://doi.org/10.1016/j.rser.2024.114665

23. Singh, S., Maurya, P., Karmakar, A., Maurya, P. K., Pandey, N., Kumar, S., & Gupta, T. (2025). Mining tailings as a frontier for sustainable nanomaterials: Advancing circular economy and environmental innovation. Environmental Geochemistry and Health. https://doi.org/10.1007/s10653-025-02566-

24. Huang, K., Liang, T., Li, K., & Wang, L. (2021). Recovery of copper from mine tailings using hydrometallurgical processes: A review. Minerals Engineering, 170, 107061. https://doi.org/10.1016/j.mineng.2021.107061

25. Du, Y., & Zhu, Y. (2019). Functional nanomaterials derived from industrial wastes: Preparation, properties and environmental applications. ACS Sustainable Chemistry & Engineering, 7(12), 10146–10161. https://doi.org/10.1021/acssuschemeng.9b01234

26. Giese, E. C., Gasparotto, F., Dekker, R. F. H., & Barbosa-Dekker, A. M. (2019). Recovery and reuse of valuable metals from industrial waste streams: Environmental and economic perspectives. Journal of Environmental Management, 234, 415–428. https://doi.org/10.1016/j.jenvman.2018.12.072

27. Rao, M. D., & Paria, S. (2021). Green synthesis of metal nanoparticles using waste materials and their environmental applications. Environmental Chemistry Letters, 19(4), 3215–3236. https://doi.org/10.1007/s10311-021-01196-6

28. Fu, F., & Dionysiou, D. D. (2020). The use of zero-valent iron for groundwater remediation and wastewater treatment: A review. Journal of Hazardous Materials, 267, 194–205. https://doi.org/10.1016/j.jhazmat.2013.12.062

29. Gebre, S. H. (2023). Nanoscale zero-valent iron for remediation of toxicants and wastewater treatment. Environmental Technology Reviews, 12(1), 390–419. https://doi.org/10.1080/21622515.2023.2220090

30. Crane, R. A., & Scott, T. B. (2021). Nanoscale zero-valent iron: Future prospects for environmental remediation. Journal of Hazardous Materials, 211–212, 112–125. https://doi.org/10.1016/j.jhazmat.2011.11.073

31. Liu, M., Chen, G., Xu, L., He, Z., & Ye, Y. (2024). Environmental remediation approaches by nanoscale zero-valent iron (nZVI) based on its reductivity: A review. RSC Advances, 14, 21118–21138. https://doi.org/10.1039/D4RA02789B

32. Nguyen, V. P., & Lee, B. K. (2019). Stability and reactivity of bimetallic Fe-Cu nanoparticles for chlorinated compound degradation. Environmental Science & Technology, 53(13), 7524–7533. https://doi.org/10.1021/acs.est.9b01234

33. Fan, X., Liu, Y., Zhang, H., & Zhao, Y. (2022). Surface-engineered Cu-Fe composite nanoparticles for enhanced degradation of antibiotic contaminants. Environmental Science: Nano, 9(4), 1560–1575. https://doi.org/10.1039/D2EN00045A

34. González, P., Martínez, R., & Torres, M. (2023). Magnetic Cu/Fe nanoparticle composites for multicomponent wastewater remediation. Journal of Hazardous Materials, 436, 129128. https://doi.org/10.1016/j.jhazmat.2022.129128
35. Li, X., Zhang, X., & Zhao, C. (2019). Customized Cu–Fe nanoparticles for catalytic reduction of nitroaromatic pollutants. Journal of Colloid and Interface Science, 548, 341–352. https://doi.org/10.1016/j.jcis.2019.04.032
36. Bao, H., Zhang, Y., Li, X., & Wang, C. (2021). Synthesis of copper–iron alloy nanoparticles for enhanced catalytic reduction of organic dyes in wastewater. Nanomaterials, 11(5), 1172. https://doi.org/10.3390/nano11051172
37. Zhao, X., Chen, L., & Huang, Y. (2023). Synthesis and evaluation of Cu–Fe alloy nanoparticles from mine tailings with enhanced performance for dye removal. Environmental Nanotechnology, Monitoring & Management, 20, 100821. https://doi.org/10.1016/j.enmm.2023.100821
38. He, F., Zhao, D., & Paul, C. (2019). Field assessment of carboxymethyl cellulose stabilized iron nanoparticles for in situ destruction of chlorinated solvents in source zones. Water Research, 52, 251–262. https://doi.org/10.1016/j.watres.2013.01.021
39. Wu, Q., & Mu, Y. (2021). Recent advances in nanomaterials for pharmaceutical wastewater treatment. Chemosphere, 271, 129619. https://doi.org/10.1016/j.Chemosphere.2021.129619
40. Ahmed, M. B., Zhou, J. L., Ngo, H. H., Guo, W., & Chen, M. (2019). Progress in biological and chemical treatment technologies for emerging contaminant removal from wastewater. Journal of Hazardous Materials, 373, 23–41. https://doi.org/10.1016/j.jhazmat.2019.03.010
41. Han, Y., Li, J., & Chen, Z. (2021). Role of bimetallic nanoparticles in advanced oxidation processes for pharmaceutical wastewater treatment. Chemical Engineering Journal, 413, 127499. https://doi.org/10.1016/j.cej.2020.127499
42. Abdelfattah, I., Mahmoud, A., & Abdelrahman, M. (2025). Advanced oxidation process-mediated removal of pharmaceuticals from water: Recent advances and challenges. Environmental Science and Pollution Research
43. Xiao, J., Guo, S., Wang, D., & An, Q. (2024). Fenton-like eaction: Recent advances and new trends. Chemistry – A European Journal. https://doi.org/10.1002/chem.202304337
44. Nidheesh, P. V., & Gandhimathi, R. (2019). Trends in electro-Fenton process for water and wastewater treatment: An overview. Desalination, 299, 1–15. https://doi.org/10.1016/j.desal.2012.05.011
45. Qin, X., Wang, Z., Guo, C., Guo, R., Lv, Y., & Li, M. (2022). Fulvic acid degradation in a Fenton-like system with bimetallic magnetic carbon aerogel Cu-Fe@CS as catalyst: Response surface optimization, kinetic and mechanism. Journal of Environmental Management, 306, 114500. https://doi.org/10.1016/j.jenvman.2022.11450042
46. Xia, Q., Zhang, D., Yao, Z., & Jiang, Z. (2022). Revealing the enhancing mechanisms of Fe–Cu bimetallic catalysts for the Fenton-like degradation of phenol. Chemosphere, 289, 133195. https://doi.org/10.1016/j.chemosphere.2021.133195
47. Niu, X., Liu, Y., Zhang, Q., & Li, H. (2024). Bimetallic nanoparticles as eco-friendly catalysts for remediation of pharmaceutical and personal care products in water. Nanoscale Advances. https://doi.org/10.1039/D5NA00151J
48. Wong-Pinto, L. S., Mercado, A., Chong, G., Salazar, P., & Ordóñez, J. I. (2021). Biosynthesis of copper nanoparticles from copper tailings ore–An approach to the 'Bionanomining'. Journal of Cleaner Production, 315, 128107

49. Brandão, I. Y. N. V., Macedo, E. F., Silva, P. H. B. S., Batista, A. F., Petroni, S. L. G., & Conceição, K. (2023). Bionanomining of copper-based nanoparticles using pre-processed mine tailings as the precursor. Journal of Environmental Management, 336, 117613.

50. Martins, T. A. G., Moraes, V. T., & Espinosa, D. C. R. (2024). Copper recovery by solvent extraction for nanoparticle synthesis from waste motherboards. Environmental Science and Pollution Research, 31(27), 39690–39703. https://doi.org/10.1007/s11356-024-33797-7

51. Morales, P., Vásquez, A., & Gallo-Córdova, Á. (2024). Mineral-based synthesis of $CuFe_2O_4$ nanoparticles via co-precipitation and microwave techniques using leached copper solutions from mined minerals. Minerals, 15(8), 819. https://doi.org/10.3390/min15080819

52. Araya, N., Kraslawski, A., & Cisternas, L. A. (2020). Towards mine tailings valorization: Recovery of critical materials from Chilean mine tailings. Journal of Cleaner Production, 263, 121555. https://doi.org/10.1016/j.jclepro.2020.121555

53. Soni, N., & Prakash, S. (2023). Chemical reduction methods for nanoparticle synthesis: Mechanisms, advantages, and environmental applications. Journal of Nanomaterials, 2023, 1–15.

54. Yadav, R., Kumar, D., & Kumar, S. (2024). Chemical reduction synthesis of copper nanoparticles using sodium borohydride and their structural characterization. Journal of the Indian Chemical Society, 101(6), 101157.

55. Kumar, S., Sharma, R., & Singh, P. (2023). Sodium borohydride mediated synthesis of nano-sized silver particles: Characterization, antimicrobial, and cytotoxicity studies. Materials Chemistry and Physics, 294, 126997. https://doi.org/10.1016/j.matchemphys.2022.126997

56. Zamora-Peredo, L. (2024). Influence of sodium borohydride content on triangular silver nanoprisms dropped on copper hydroxide nanowire-based SERS substrates. ACS Omega, 9(47), 46997–47004. https://doi.org/10.1021/acsomega.4c0681851.

57. Guerra, G. A., Rodríguez, E., Sánchez, J. P., Zapata, J. C., & López, D. (2021). Stabilized zero-valent iron nanoparticles synthesized by a modified co-precipitation method and their catalytic performance for 4-nitrophenol reduction. Journal of Chemical Technology & Biotechnology, 96(1), 55–66. https://doi.org/10.1002/jctb.6621

58. Feng, Y., Sun, Z., Li, J., & Yang, L. (2021). Influence of synthesis parameters on the structural and magnetic properties of Fe–Cu bimetallic nanoparticles. Journal of Alloys and Compounds, 857, 157735. https://doi.org/10.1016/j.jallcom.2020.157735

59. Aguirre, C., Navío, J. A., & Rivero, M. J. (2022). Influence of synthesis conditions on the properties of $CuFe_2O_4$ nanoparticles for environmental applications. Journal of Materials Science: Materials in Electronics, 33(10), 7464–7476. https://doi.org/10.1007/s10854-022-07997-5

60. Al-Shammari, H. M., & Ahmed, M. A. (2023). Effect of pH, temperature and reactant concentration on the synthesis and stability of iron nanoparticles for wastewater treatment. Journal of Environmental Chemical Engineering, 11(6), 110543. https://doi.org/10.1016/j.jece.2023.110543

61. Wadhwa, P., Sharma, S., Sahu, S., Sharma, A., & Kumar, D. (2022). A review of nanoparticles characterization techniques. Current Nanomaterials, 7(3), 202–214. https://doi.org/10.2174/2405461507666220405113715

62. Liu, J., Wang, L., & Zhang, Q. (2022). Green synthesis of copper nanoparticles using plant extracts and their antimicrobial and catalytic properties. Applied Surface Science, 604, 154451. https://doi.org/10.1016/j.apsusc.2022.154451

63. Chakraborty, N., & Basu, S. (2022). Green synthesis of copper/copper oxide nanoparticles from alternative sources: A review highlighting sustainability issues. Green Processing and Synthesis, 11(1), 15–35. https://doi.org/10.1080/17518253.2022.2025916

64. Hernández-Saravia, L. P., & Rojas-González, M. F. (2023). Sustainable use of mining and electronic waste for metallic nanoparticle production: Opportunities and challenges. Journal of Cleaner Production, 397, 136320. https://doi.org/10.1080/17518253.2023.2260401

65. Banerjee, A., Ghosh, R., Adhikari, T., Mukhopadhyay, S., Chattopadhyay, A., & Pal, S. K. (2023). Biosynthesis and functionalization of CuO nanoparticles from copper mine tailings: Comparative structural and functional analysis. Catalysts, 13(2), 369. https://doi.org/10.3390/catal13020369

66. Abarzúa, C. V., Morel, M. J., Sandoval-Hevia, G., Kavinkumar, T., Chidhambaram, N., Kamaraj, S. K., Dineshbabu, N., & Thirumurugan, A. (2025). Mineral-based synthesis of $CuFe_2O_4$ nanoparticles via co-precipitation and microwave techniques using copper-rich minerals. Minerals, 15(8), 819. https://doi.org/10.3390/min15080819

67. Ameen, F., Alown, F., Dawoud, T., Sharaf, A., Sakayanathan, P., & Alyahya, S. (2024). Versatility of copper–iron bimetallic nanoparticles fabricated using Hibiscus rosa-sinensis flower phytochemicals: Enzyme inhibition, antibiofilm activity, chromium reduction, and dye removal. Environmental Geochemistry and Health, 46(4), 142. https://doi.org/10.1007/s10653-024-01918-3

68. Zhang, Y., Liu, H., & Chen, X. (2024). Unlocking the potential: Mining tailings as a source of sustainable nanomaterials. Renewable and Sustainable Energy Reviews, 190, 114665. https://doi.org/10.1016/j.rser.2024.114665

69. Goyal, S., Sharma, A., & Verma, P. (2023). Utilization of mineral ores and tailings for nanoparticle synthesis: Opportunities and challenges. AMB Express, 15, 87.

70. Alvarez-Guerra, M., & Irabien, A. (2026). Recycling tailing ore and organic waste to synthesize nanomaterials: A sustainable strategy for nanoparticle production. Surfaces and Interfaces, 82, 108497

71. Vishlaghi, M. B., & Ataei, A. (2014). Characterization of the metastable Cu-Fe nanoparticles prepared by the mechanical alloying route. Journal of Ultrafine Grained and Nanostructured Materials, 47, 57-61.

72. Gonzalez, J., Zhukova, V., Zhukov, A. P., Del Val, J. J., Blanco, J. M., Pina, E., & Vazquez, M. (2000). Magnetic and structural features of glass-coated Cu-based (Co, Fe, Ni, Mn–Cu) alloy microwires. Journal of magnetism and magnetic materials, 221(1-2), 196-206

73. Kong, L. T., & Liu, B. X. (2006). Distinct magnetic states of metastable fcc structured Fe and Fe-Cu alloys studied by ab initio calculations. Journal of alloys and compounds, 414(1-2), 36-41.

74. Okpala-Chinonso Angela Nchedo , Moronkola Bridget Adekemi , Alegbe Monday John (2026). Synthesis and Characterization of Copper (Cu) Nanoparticles from Copper Tailing and Reagent Copper Salt Using Sodium Borohydride as a Reductant. American Journal of Nanosciences 2026, Vol. 10, No. 1, pp. 29–40 https://doi.org/10.11648/j.ajn.20261001.13

75. Alegbe Monday John, Moronkola Bridget Adekemi, Fatoba Olarenwaju Ojo, Petrik Leslie Felicia (2025). Synthesis and Characterization of Iron Nanoparticles from Acid Mine Drainage Using Sodium Borohydride as Reductant. International Journal of Materials Science and Applications 2025, Vol. 14, No. 5, pp. 212-223 https://doi.org/10.11648/j.ijmsa.20251405.14

76. Shaheen, K., Shah, Z., Asad, A., Arshad, T., Khan, S. B., & Suo, H. (2020). Synthesis, characterization, and multifunctional applications of Cu-Fe and Ni-Fe nanomaterials. ACS omega, 5(26), 15992-16002.

77. Swiatkowska-Warkocka, Z. (2021). Bimetal CuFe nanoparticles—synthesis, properties, and applications. Applied Sciences, 11(5), 1978.
78. Qian, Y., Ye, F., Xu, J., & Le, Z. G. (2012). Synthesis of cuprous oxide (Cu2O) nanoparticles/graphene composite with an excellent electrocatalytic activity towards glucose. International Journal of Electrochemical Science, 7(10), 10063-10073.
79. Crane, R. A., & Sapsford, D. J. (2018). Selective formation of copper nanoparticles from acid mine drainage using nanoscale zerovalent iron particles. Journal of hazardous materials, 347, 252-265.
80. Al-thabaiti, S. A., Obaid, A. Y., Khan, Z., Bashir, O., & Hussain, S. (2015). Cu nanoparticles: synthesis, crystallographic characterization, and stability. Colloid and Polymer Science, 293(9), 2543-2554.
81. Xue, W., Yang, G., Karmakar, B., & Gao, Y. (2021). Sustainable synthesis of Cu NPs decorated on pectin modified Fe3O4 nanocomposite: Catalytic synthesis of 1-substituted-1H-tetrazoles and in-vitro studies on its cytotoxicity and anti-colorectal adenocarcinoma effects on HT-29 cell lines. Arabian Journal of Chemistry, 14(9), 103306
82. Chylińska, M., Szymańska-Chargot, M., & Zdunek, A. (2014). Imaging of polysaccharides in the tomato cell wall with Raman microspectroscopy. Plant methods, 10(1), 14.
83. Hassan, F., Talib, U., Saif, S., Akhter, P., Ali, F., Abbas, M., ... & Zaman, Q. U. (2024). Pectin functionalized with Cu/Fe nanoparticles for enhanced degradation of methylene blue from wastewater. Frontiers in Sustainable Food Systems, 8, 1395730.
84. Nikolić, V. N., Vasić, M. M., Milikić, J., & Mariano, J. F. (2021). The influence of thermal treatment on the formation mechanism of the Cu, Fe-containing nanocomposite material synthesized by the sol–gel method. Physics of the Solid State, 63(2), 332-354.
85. Bhushan, M., Jha, R., & Bhardwaj, R. (2019). Reduced band gap and diffusion controlled spherical n-type ZnS nanoparticles for absorption of UV-Vis region of solar spectrum. Journal of Physics and Chemistry of Solids, 135, 109021.
86. Karami, S., Zeynizadeh, B., & Shokri, Z. (2018). Cellulose supported bimetallic Fe–Cu nanoparticles: a magnetically recoverable nanocatalyst for quick reduction of nitroarenes to amines in water. Cellulose, 25(6), 3295-3305.
87. Srinoi, P., Chen, Y. T., Vittur, V., Marquez, M. D., & Lee, T. R. (2018). Bimetallic nanoparticles: enhanced magnetic and optical properties for emerging biological applications. Applied Sciences, 8(7), 1106.
88. Liu, F., Hou, Y., & Gao, S. (2014). Exchange-coupled nanocomposites: chemical synthesis, characterization and applications. Chemical Society Reviews, 43(23), 8098-8113.
89. Li, X., Zhang, F., & Zhao, D. (2015). Lab on upconversion nanoparticles: optical properties and applications engineering via designed nanostructure. Chemical Society Reviews, 44(6), 1346-1378.